BIOCHEMISTRY
including biophysical chemistry & molecular biology

Article

pubs.acs.org/biochemistry

Impact of Calcium Binding and Thionylation of S100A1 Protein on Its Nuclear Magnetic Resonance-Derived Structure and Backbone Dynamics

Michał Nowakowski,*[,†,∥] Katarzyna Ruszczyńska-Bartnik,[†] Monika Budzińska,[†] Łukasz Jaremko,[†,‡,⊥] Mariusz Jaremko,[†,⊥] Konrad Zdanowski,[†,§] Andrzej Bierzyński,[†] and Andrzej Ejchart[†]

[†]Institute of Biochemistry and Biophysics, Polish Academy of Sciences, Pawińskiego 5A, 02-106 Warsaw, Poland

[‡]Faculty of Chemistry, Warsaw University, Pasteura 1, 02-093 Warsaw, Poland

[§]Institute of Chemistry, University of Natural Sciences and Humanities, 3 Maja 54, 08-110 Siedlce, Poland

Supporting Information

ABSTRACT: S100 proteins play a crucial role in multiple important biological processes in vertebrate organisms acting predominantly as calcium signal transmitters. S100A1 is a typical representative of this family of proteins. After four Ca^{2+} ions bind, it undergoes a dramatic conformational change, resulting in exposure, in each of its two identical subunits, a large hydrophobic cleft that binds to target proteins. It has been shown that abnormal expression of S100A1 is strongly correlated with a number of severe human diseases: cardiomyopathy and neurodegenerative disorders. A few years ago, we found that thionylation of Cys 85, the unique cysteine in two identical S100A1 subunits, leads to a drastic increase of the affinity of the protein for calcium. We postulated that the protein activated by thionylation becomes a more efficient calcium signal transmitter. Therefore, we decided to undertake, using nuclear magnetic resonance methods, a comparative study of the structure and dynamics of native and thionylated human S100A1 in its apo and holo states. In this paper, we present the results obtained for both forms of this protein in its holo state and compare them with the previously published structure of native apo-S100. The main conclusion that we draw from these results is that the increased calcium binding affinity of S100A1 upon thionylation arises, most probably, from rearrangement of the hydrophobic core in its apo form.

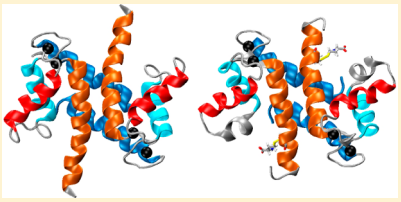

A large number of papers on the structure and biological function of S100 proteins can be found in the literature, and every year this number increases dramatically. There is a good reason for this: these proteins, acting predominantly as calcium signal transmitters, have been shown to play a crucial role in multiple important biological processes in vertebrate organisms.[1]

S100A1 is a typical S100 protein. It is a homodimer composed of noncovalently bound, antiparallel oriented, subunits. Each of them consists of two so-called "EF-hand" motifs bound together by a short linker. The N-terminal motifs contain a 14-residue calcium binding loop, specific for S100 proteins, flanked by two α-helices (helix I and helix II). The C-terminal ones coordinate Ca^{2+} ions by a "canonical" loop, ubiquitous in calcium binding proteins, formed by 12 amino acid residues situated between helix III and helix IV.

Once Ca^{2+} binds, the protein undergoes a dramatic conformational change, resulting in exposure, in each of its subunits, a large hydrophobic cleft formed by residues situated in the linker, the C-terminus, and helix III.[2] Numerous structural studies indicate that this region is responsible for recognition of S100 target proteins.[3]

S100A1 is strongly expressed in human heart muscle and brain. It is also found in skeletal muscles and kidney. It has been shown that abnormal expression of this protein is strongly correlated with a number of severe human diseases: cardiomyopathy and neurodegenerative disorders such as Alzheimer's disease.[4−7]

A few years ago, we found that thionylation of Cys 85 (the strictly conserved, unique cysteine residue of S100A1 subunits) by small thiol molecules such as β-mercaptoethanol, glutathione, or cysteine leads to a dramatic increase in the affinity of the protein for calcium.[8] It prompted us to formulate the hypothesis that S100A1 can play the role of a linker between calcium and redox signal pathways.

Protein S-thionylation is the posttranslational modification of cysteine residues that occurs via formation of a mixed disulfide between the cysteine thiol group and low-molecular mass endogenous thiols. At present, a large number of proteins undergoing thionylation have been described.[9] Thionylation of proteins has been shown to regulate activities of enzymes, transcriptional factors, cell surface receptors, and cytoskeletal proteins. It plays an essential part in the control of cell signaling pathways associated with viral infections and with tumor necrosis factor.[10] The thionylation has been also suggested as a

Received: November 15, 2012
Revised: January 25, 2013
Published: January 25, 2013

dx.doi.org/10.1021/bi3015407 | *Biochemistry* 2013, 52, 1149−1159

mechanism through which protein functions can be regulated by the redox status.[11]

To elucidate the molecular mechanism of S100A1 activation due to thionylation, we decided to undertake, using nuclear magnetic resonance (NMR) methods, a precise comparative study of the structure and dynamics of human S100A1 protein, native and with a thionylated Cys 85 residue, in its apo and holo states.

Knowledge of static three-dimensional (3D) structures of proteins, while extremely important, is not sufficient to fully understand the function of proteins and their interactions in complexes. It is believed that intramolecular motions in proteins are one of the most important factors that determine their basic physicochemical properties, biological activity, and also interactions with ligands, receptors, or nucleic acids. Magnetic relaxation of ^{15}N amide nuclei allows one to monitor motions of protein backbone over a wide range of time scales. This approach of probing dynamics of NH groups allows characterization of motions over most of the protein backbone.[12,13]

The results obtained by us for human apo-S100A1 have already been published.[14] In the work presented here, we discuss the structure and dynamics of the holo form of this protein and its mixed disulfide with homocysteine.

The choice of homocysteine can seem rather puzzling: glutathione is by far the most abundant thiol molecule in vertebrate organisms and, therefore, the most likely to form mixed disulfides with proteins. On the other hand, homocysteine is situated at a critical regulatory branch point in sulfur metabolism. It can be remethylated to methionine, an important amino acid in protein synthesis, or converted to cysteine in the transsulfuration pathway.[15] It has been shown that homocysteine has the strongest tendency to create disulfide bonds with proteins among such thiols as homocysteine, cysteine, and glutathione in HeLa cell cultures. Such S-homocysteinylation impairs the function of many enzymes, structural proteins, and receptors, disturbing many metabolic functions in the cell.[16] It has been also shown that homocysteine administered orally resulted in the increase in the level of protein-bound homocysteine in plasma with a concurred decrease in protein-bound cysteine, suggesting displacement of bound cysteine.[17] An elevated level of homocysteine is associated with an increased risk of cardiovascular disease,[18] cerebrovascular disease, Alzheimer's disease, neural tube defects, osteoporosis, renal failure, and diabetes. Homocysteine can form mixed disulfides with plasma proteins, such as albumin, transthyretin, fibronectin, or lipoprotein(a) as well as with intracellular proteins like metallothionein or glutathione peroxidase.[19] Therefore, homocysteinylation of S100A1, while not reported yet, might be a biologically important phenomenon: high levels of homocysteine are considered to be risk factors in the same disorders that are linked with abnormal S100A1 expression.[20,21]

MATERIALS AND METHODS

Sample Preparation. ^{15}N-labeled S100A1 protein and doubly ^{13}C- and ^{15}N-labeled S100A1 protein were obtained as previously described.[14,22] Expression products were isolated using the classical method of ammonium sulfate precipitation,[23,24] purified by reversed-phase HPLC on a semi-preparative Vydac C18 column, and identified by electrospray ionization mass spectrometry using a Macromass Q-Tof spectrometer. Two forms of the protein, one with the sequence strictly corresponding to its gene sequence and another one, with the additional initiator methionine at the N-terminus, were obtained via HPLC as partly overlapping peaks. NMR measurements indicated that structural differences between both forms are small and restricted to the proximity of the N-terminal Met residue.[14,25] Therefore, a mixture of both forms of proteins was used in all experiments. Thionylation of S100A1 protein with homocysteine (formation of a disulfide bond between Cys 85 and homocysteine, S100A1-Hcy) was performed in 0.2 M Tris buffer containing 5 M GuHCl, 5 mM EDTA, and 5 mM homocystine disulfide (pH 8.5). The reaction was conducted at room temperature for 50 min. The modified protein was purified by HPLC and identified by electrospray ionization mass spectrometry. NMR samples with a volume of 650 μL contained a 0.8−1.0 mM protein solution (monomer concentration) in a 90:10 H_2O/D_2O mixture, 50 mM Tris-d_{11}, 10 mM $CaCl_2$, 0.1 mM NaN_3, and 50 mM NaCl, with the pH adjusted to 7.2 (uncorrected value). In the case of H_C-detected experiments, 100% deuterated buffer was used.

NMR Spectroscopy. All NMR measurements were performed at the carefully adjusted temperature of 37 °C, which was checked by an ethylene glycol reference sample. Time domain data were acquired using States−TPPI quadrature detection[26] followed by the sensitivity-enhanced detection introduced by L. E. Kay.[27] A 1.6 s recycling delay was used, if not stated otherwise. All chemical shifts in ^{1}H NMR spectra were reported with respect to external DSS-d_4. Chemical shifts of ^{13}C and ^{15}N signals were referenced indirectly using the 0.251449530 and 0.101329118 frequency ratios for ^{13}C/^{1}H and ^{15}N/^{1}H, respectively.[28] Experimental data were processed using NMRPipe.[29] Zero filling and a 90°-shifted squared sine-bell filter were applied prior to Fourier transformation. Processed spectra were analyzed with both CARA[30] and SPARKY.[31]

The sequence-specific assignments were performed using uniformly doubly ^{13}C- and ^{15}N-labeled samples of holo-S100A1 and holo-S100A1-Hcy. 3D heteronuclear HNCO,[32] HNCA,[33] HN(CO)CA,[34] HNCACB,[35] CBCA(CO)NH,[36] and (HCA)-CO(CA)NH[37] spectra were used to obtain assignments of the backbone ^{1}H, ^{13}C, and ^{15}N resonances. The assignments were additionally confirmed by analysis of sequential and medium-range nuclear Overhauser effect (NOE) signals in the respective 3D ^{15}N-edited NOESY-HSQC spectra.[38] The aliphatic side chain ^{1}H and ^{13}C resonances were assigned from the analysis of the ^{1}H−^{13}C HSQC, C(CO)NH,[39] HBHA(CBCACO)NH,[40] HCCH-TOCSY,[41] (H)CCH-TOCSY,[41] and ^{13}C-edited NOESY-HSQC spectra.[42] The aromatic side chain resonances were assigned from the (HB)CBHD, (HB)CBHE,[43] ^{1}H−^{13}C HSQC, and ^{13}C-edited NOESY-HSQC spectra recorded with the offset, spectral widths, and ^{13}C−^{1}H coupling constants tuned to aromatic carbons. Distance constraints were obtained from the ^{15}N-edited NOESY-HSQC spectra and the ^{13}C-edited NOESY-HSQC spectra separately tuned to aliphatic and aromatic carbons.

Longitudinal (R_1) and transverse (R_2) relaxation rates were measured at three magnetic fields (9.4, 11.7, and 16.4 T), with the ^{15}N-labeled sample using the sensitivity-enhanced ^{1}H−^{15}N HSQC pulse sequence[27] with the option of either R_1 or R_2 measurements of ^{15}N nuclei.[44] The R_2 relaxation rate measurements were performed with the CPMG pulse train. A refocusing time of 650 μs was used during the evolution delays. The acquisition parameters for R_1 and R_2 measurements on

dx.doi.org/10.1021/bi3015407 | Biochemistry 2013, 52, 1149−1159

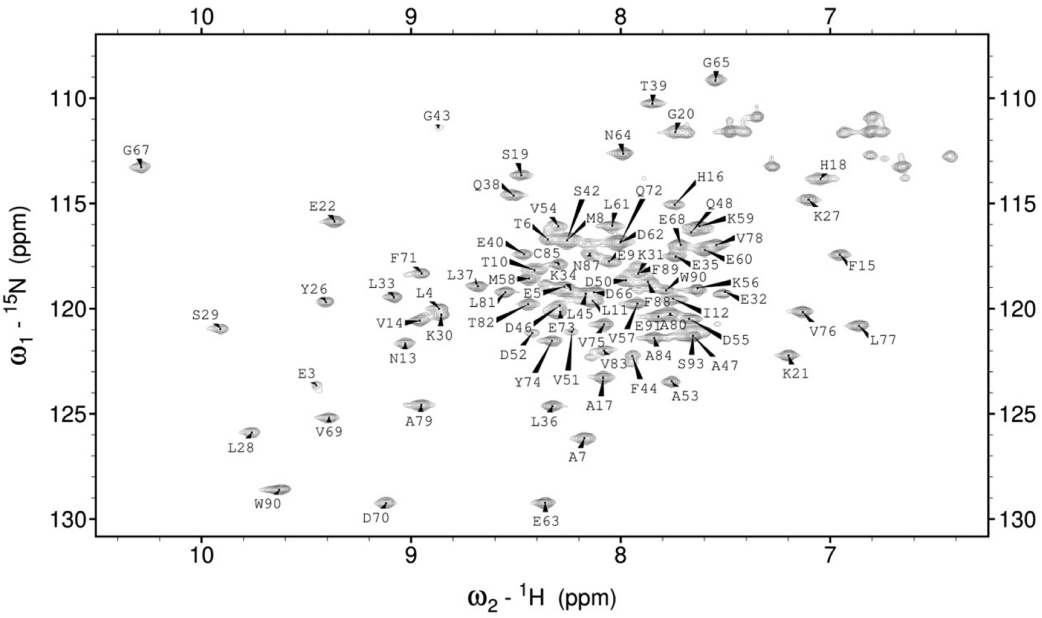

Figure 1. $^{1}H-^{15}N$ HSQC spectrum of human holo-S100A1 protein. The terminal NH_2 groups of Asn and Gln residues are not labeled. One of two cross-peaks labeled W90 at 9.621 and 128.53 corresponds to the side chain NH group of the indole moiety.

each spectrometer were identical with the exception of the delay between π (^{1}H) pulses used for cross-correlation effect suppression.[45] Delays of 5 and 10 ms were used in the R_1 and R_2 measurements, respectively. Delays between the scans of 1.8 s were employed in both types of experiments. $\{^{1}H\}-^{15}N$ NOEs were measured with the pulse sequence included in ProteinPACK (Varian Inc., Palo Alto, CA) at 16.4 T for holo-S100A1 and 9.4 and 16.4 T for holo-S100A1-Hcy.

Resonance intensities were used in calculating relaxation rates and NOE values. Experimental errors of relaxation rates were obtained from appropriate elements of the variance–covariance matrix. Experimental errors in NOE values were evaluated from signal-to-noise ratios obtained for corresponding signals in spectra with and without NOEs.[46]

The ^{1}H, ^{13}C, and ^{15}N resonance assignments and ^{15}N magnetic relaxation data have been deposited in the BioMagResBank as entries 18231 (holo-S100A1) and 18230 (holo-S100A1-Hcy).

Structure Calculations. The NOESY interproton distance constraints were derived from the 3D heteronuclear ^{15}N- and ^{13}C-edited NOESY-HSQC experiments. The initial structure calculations were performed with CYANA version 3.0.[47] The dimeric interface between the protein subunits was defined on the basis of structural similarity to the known structure of rat S100A1 protein[2] [Protein Data Bank (PDB) entry 1ZFS]. The automatic NOESY assignment procedure[48] provided 1193 intrasubunit distance constraints and 121 intersubunit distance constrains for holo-S100A1 protein. Appropriate numbers for holo-S100A1-Hcy were 1240 and 156, respectively. Stereospecific assignments for 74 (holo-S100A1) or 100 (holo-S100A1-Hcy) side chain chiral groups in each subunit were generated with GLOMSA,[49] which is included in CYANA. Additional restraints for backbone φ and ψ torsion angles for the Ser 2–His 18, Leu 28–Glu 63, and Val 69–Thr 82 segments were predicted from the chemical shifts using the PREDITOR server.[50] For the less defined protein regions (like Ser 19–Lys 27 and Asn 64–Glu 68 calcium binding loop segments or the C-terminus of helix IV starting from Val 83), the dihedral angle constraints were not applied. At first, the structure calculations were conducted using XPLOR-NIH 2.26[51] with NOEs and dihedral angles as input constraints assuming symmetry equivalence between two subunits. Before the final structure calculations, constraints defined as r_{HN-O} = 1.5–2.5 Å and r_{N-O} = 2.5–3.5 Å for hydrogen bonds were added on the basis of geometric criteria. If a given hydrogen bond existed in more than 75% of the structures in the ensemble, then it was selected for the final refinement. Twenty additional constrains, defined as $r_{Ca^{2+}-O}$ = 2.33–2.47 Å for calcium ion coordination, were also included in the final refinement. Only oxygen atoms taking part directly in calcium coordination were selected (O of Ser 19, Glu 22, Asp 24, and Lys 27 and OE1 and OE2 of Glu 32 for the first binding site and OD1 of Asp 62 and Asn 64, OD1 and OD2 of Asp 66, O of Glu 68, and OE1 and OE2 of Glu 73 for the second binding site), on the basis of the representative crystallographic structures of human S100A13 (PDB entry 2EGD) and bovine S100B (PDB entry 1MHO). For the purpose of the final refinement of the holo-S100A1-Hcy structure, the topology of an additional amino acid, homocysteine connected to cysteine by a disulfide bond, was manually added and included in the XPLOR-NIH 2.26 topology file. Evaluation of the quality of the obtained S100A1 structures was conducted with PROCHECK-NMR[52] and What-If.[53]

Analysis of ^{15}N Relaxation Data. The methodology of analyzing ^{15}N relaxation data measured at multiple magnetic fields has been described previously.[14] It is based on the extended model-free approach[54] with spectral density functions combined[55,56] with anisotropic overall tumbling.[57]

Three Euler angles relate the directions of the principal axes of the asymmetric diffusion tensor to the molecule-fixed coordinate system. Because of the symmetry requirement, one of the principal axes of the diffusion tensor of homodimeric S100A1 protein (in our case the z axis) is collinear with the protein symmetry axis. This condition reduces the number of the Euler angles from three to one. The coefficients describing the orientation of H–N vectors in the molecule-fixed

dx.doi.org/10.1021/bi3015407 | Biochemistry 2013, 52, 1149–1159

Table 1. NMR-Derived Constraints and Statistics for Human Holo-S100A1 and Holo-S100A1-Hcy Proteins Calculated with XPLOR-NIH 2.26

no. of NOE distance constraints within the subunit	1193	1240
intraresidual and sequential ($\|i-j\| \leq 1$)	713	723
medium-range ($1 < \|i-j\| < 5$)	302	270
long-range ($\|i-j\| \geq 5$)	178	247
no. of intersubunit NOE distance constraints per subunit	121	158
hydrogen bond constraints	29	50
restraints per residue	14.4	15.6
restraints for Ca^{2+} ion per subunit	10	10
torsion angle constraints		
backbone (φ/ψ)	74/71	67/67
side chains (χ^1/χ^2)	0/0	0/0
mean rmsd from experimental restraints (±SD)		
NOE (Å)	0.0126 ± 0.0012	0.0192 ± 0.0013
dihedral angles (deg)	1.13 ± 0.20	0.59 ± 0.08
rmsd from idealized covalent geometry (region 1−93) (±SD)		
bonds (Å)	0.0038 ± 0.0003	0.0056 ± 0.0003
angles (deg)	0.68 ± 0.03	0.84 ± 0.02
impropers (deg)	0.56 ± 0.03	0.65 ± 0.02
Ramachandran plot (1−93)		
residues in the most favored regions (%)	95.1	95.9
residues in additional allowed regions (%)	4.1	3.7
residues in generously allowed regions (%)	0.6	0.2
residues in disallowed regions (%)	0.2	0.2
Ramachandran plot (5−85)		
residues in the most favored regions (%)	94.4	95.7
residues in additional allowed regions (%)	4.6	4.0
residues in generously allowed regions (%)	0.7	0.1
residues in disallowed regions (%)	0.3	0.2
rmsd from the mean subunit structure		
ordered backbone atoms (1−93) (Å)	1.06 ± 0.25	0.84 ± 0.20
ordered heavy atoms (1−93) (Å)	1.70 ± 0.26	1.19 ± 0.17
ordered backbone atoms (5−85) (Å)	0.86 ± 0.22	0.44 ± 0.10
ordered heavy atoms (5−85) (Å)	1.49 ± 0.26	0.85 ± 0.12
rmsd from the mean structure of the whole dimer (both subunits)		
ordered backbone atoms (1−93) (Å)	1.17 ± 0.29	0.89 ± 0.20
ordered heavy atoms (1−93) (Å)	1.78 ± 0.29	1.13 ± 0.17
ordered backbone atoms (5−85) (Å)	0.94 ± 0.22	0.54 ± 0.14
ordered heavy atoms (5−85) (Å)	1.54 ± 0.27	1.04 ± 0.15
structure Z scores		
first-generation packing quality	2.081 ± 0.525	2.088 ± 0.451
second-generation packing quality	4.573 ± 1.451	3.885 ± 1.278
Ramachandran plot appearance	1.687 ± 0.364	1.954 ± 0.319
χ^1 and χ^2 rotamer normality	2.010 ± 0.438	0.369 ± 0.412
backbone conformation	0.647 ± 0.504	−0.181 ± 0.200
equivalent X-ray resolution of the Ramachandran plot (1−93) (Å)	1.0	1.0
equivalent X-ray resolution of the Ramachandran plot (5−85) (Å)	1.0	1.0
equivalent X-ray resolution of χ^1 and χ^2 (1−93) (Å)	1.0/1.0	1.1/1.0

coordinate system were calculated using the atomic coordinates of the lowest-energy NMR-derived structures. The vibrationally averaged N−H distance was assumed to be 0.104 nm[58] and the chemical shift anisotropy of the ^{15}N chemical shift tensor equal to −170 ppm.[59] The values and ratios of the principal values of inertia tensors are given in Table S1 of the Supporting Information and compared with those of apo-S100A1. Anisotropies of the inertia moment tensors are noticeable, and therefore, anisotropic overall tumbling may be expected.

The least-squares procedure used a Fortran routine written in-house optimizing the model parameters that consisted of minimization through a grid search of target function χ given by

$$\chi = \sum_{i=1}^{N}\sum_{j=1}^{M}[(P_{ij,\mathrm{exp}} - P_{ij,\mathrm{calc}})^2/\sigma_{ij}{}^2]$$

The sum was over M relaxation parameters for each of N residues, and $P_{ij,\mathrm{calc}}$ values were the appropriate relaxation parameters calculated from the assumed model. The σ_{ij} values were the corresponding standard deviations of experimentally derived $P_{ij,\mathrm{exp}}$ values. The minimization procedure delivered four global parameters (three diffusion coefficients and one Euler angle) and N sets of local, residue-specific, parameters comprising S_f, S_s, τ_f, τ_s, and R_{ex}. The residues of both flexible termini were also excluded from the calculation, which yielded

dx.doi.org/10.1021/bi3015407 | Biochemistry 2013, 52, 1149−1159

the overall diffusion parameters. Those unstructured, flexible terminal segments cannot be regarded as a part of the rigid rotor, and description of their motions in terms of a single overall correlation time does not seem to be appropriate.[60,61] Model parameter uncertainties derived in the minimization of target function χ were obtained as standard deviations from 200 Monte Carlo simulations.[62]

RESULTS

Sequence-Specific Resonance Assignment. The two-dimensional (2D) $^{1}H-^{15}N$ HSQC spectra of both homodimeric S100A1 proteins displayed relatively good dispersion of amide correlation signals (cf. Figure 1). In holo-S100A1-Hcy, cross-peaks for all residues could be assigned, except for those of five residues placed at the N-terminus (Ser 2), the N-binding loop (Gly 23, Asp 24, and Lys 25), and the linker (Lys 49). In holo-S100A1, the cross-peaks of the same residues and additionally of three others (Leu 41, Asn 86, and Asn 92) could not be identified because of line broadening caused, most probably, by exchange processes. The sequence-specific backbone and side chain assignments were made using 2D and 3D NMR experiments; 91.4% of all resonances in holo-S100A1 and 89.8% in holo-S100A1-Hcy were assigned. All resonances, except those of histidine rings and NH_2 side chain groups of asparagines and glutamines, have been assigned unequivocally. The $^{13}C_\beta$ chemical shift of Cys 85 in holo-S100A1-Hcy (δC_β = 40.6), as compared with that in holo-S100A1 (δC_β = 26.5), clearly shows that the protein was thionylated,[63,64] but the resonance assignment for the unlabeled homocysteine was not possible.

Effect of Calcium Binding on the $^{1}H-^{15}N$ HSQC Spectrum of S100A1. It is well-known that saturation with calcium changes significantly many of the chemical shifts in S100 proteins.[2] In human S100A1, prominent examples are those of Glu 63 and Gly 67 occupying the positions 2 and 6, respectively, of the "canonical" calcium-binding loop. Their cross-peaks in the $^{1}H-^{15}N$ HSQC spectrum move from 118.86 and 8.09 ppm and 109.02 and 8.22 ppm[14] to 129.19 and 8.35 ppm and 113.25 and 10.27 ppm (this paper), respectively, upon calcium binding. Coordination of Ca^{2+} ions by S100A1 is also manifested by more general changes in the chemical shifts of the protein backbone amide nuclei in the $^{1}H-^{15}N$ HSQC spectra upon saturation of the apoprotein with calcium ions. The chemical shift perturbation (CSP) upon binding of Ca^{2+} ions was calculated for each residue using the equation $CSP = [(\Delta\delta_{HN})^2 + (0.2\Delta\delta_N)^2]^{1/2}$, where $\Delta\delta_{HN}$ and $\Delta\delta_N$ are chemical shift changes in proton and nitrogen dimensions, respectively. CSP values are shown in Figure S1 of the Supporting Information. The largest changes are observed for both binding loops. Pronounced changes are also visible for the linker, particularly for its first residue, Ser 42, and the C-terminal part of helix IV. On average, CSPs equal 0.69 ppm for both pairs (apo-S100A1 with holo-S100A1 and apo-S100A1 with holo-S100A1-Hcy). Both CSP profiles mapped onto appropriate protein structures are given in Figure S2 of the Supporting Information. A similar calcium-induced chemical shift perturbation profile was observed in the case of human S100A5 protein.[65]

Structures of Holo-S100A1 and Holo-S100A1-Hcy. The 3D solution structures of the human holo-S100A1 protein and its derivative modified by disulfide formation with homocysteine at Cys 85 (holo-S100A1-Hcy) were calculated from NMR-derived constraints (cf. Table 1); 99.2% (99.6%) of all residues are located in the most favored [95.1% (95.9%)] or additionally allowed [4.1% (3.7%)] regions of the Ramachandran plot. The statistics for the ensembles of the 20 most favorable structures for both proteins are listed in Table 1. In Figure 2, the ribbon diagrams for the lowest-energy structures

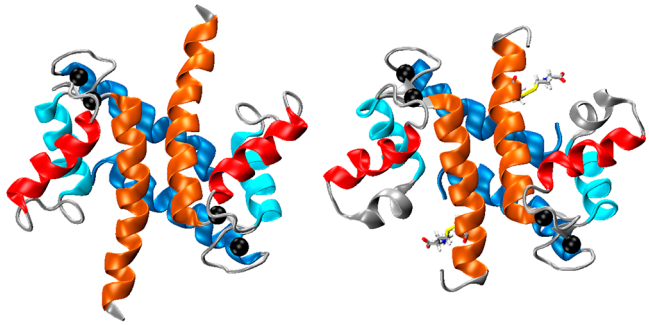

Figure 2. Ribbon representations of the holo-S100A1 (A) and holo-S100A1-Hcy (B) structures. Subsequent helices of EF-hand motifs are colored blue (helix I), cyan (helix II), red (helix III), and yellow (helix IV). Calcium ions are shown as spheres, and homocysteine is shown as sticks.

of holo-S100A1 (Figure 2A) and holo-S100A1-Hcy (Figure 2B) are shown with color-encoded EF-hand helices. The atomic coordinates for all 20 structures of each protein have been deposited in the Protein Data Bank as entries 2LP3 for human holo-S100A1 and 2LP2 for holo-S100A-Hcy.

The structures of both proteins are almost identical, as could be expected from comparison of their $^{1}H-^{15}N$ HSQC spectra: the average chemical shift perturbation CSP for the pair of holo-S100A1 and holo-S100A-Hcy equals merely 0.04 ppm (cf. Figure S1C of the Supporting Information), and it arises predominantly from local effects of protein thionylation. Each subunit of holo-S100A1 (holo-S100A1-Hcy) contains four α-helices formed by residues Glu 3−Gly 20 (Lys 21), Lys 30−Glu 40, Ala 53−Leu 61, and Phe 71−Glu 91 (Trp 90) and one short antiparallel β-sheet formed by Lys 27, Leu 28, Val 69, and Asp 70. In the linker region joining two EF-hand domains (residues 41−50) of holo-S100A1-Hcy, the α-helix consists of Gly 43−Asp 46. Such a short helical motif does not appear in holo-S100A1 proteins of either the human (this work) or the rat[2] species.

For residues Glu 5−Cys 85 within one subunit of holo-S100A1 (holo-S100A1-Hcy), the rmsd for the backbone atoms (N, C_α, and C′) equals 0.86 ± 0.22 Å (0.44 ± 0.10 Å) and for all heavy atoms 1.49 ± 0.26 Å (0.85 ± 0.12 Å), while for both subunits in the dimer, the corresponding values are 0.94 ± 0.22 Å (0.54 ± 0.14 Å) and 1.54 ± 0.27 Å (1.04 ± 0.15 Å), respectively. Almost identical rmsd values obtained for the single subunit and the homodimer in both proteins prove that the interface between subunits is correctly determined and the resulting ensembles of structures represent well-defined homodimeric proteins. In both proteins, the dimer interface is located mainly between helices I and I′, helices I and IV′, and helices IV and IV′. On average, four or five long-range distance restraints have been established from the NOE data for residues involved in dimer formation.

Dynamics of Holo-S100A1 and Holo-S100A1-Hcy. For holo-S100A1 and holo-S100A1-Hcy proteins, the analysis of relaxation data was performed for 73 and 66 residues, respectively, allowing for the simultaneous determination of

dx.doi.org/10.1021/bi3015407 | Biochemistry 2013, 52, 1149−1159

four global parameters and corresponding sets of local parameters. The principal values of the overall diffusion tensors are listed in Table S2 of the Supporting Information. As supposed, the overall tumbling is anisotropic with anisotropy $D_A = 2D_z/(D_x + D_y)$ equal to 0.78 ± 0.01 and 0.88 ± 0.04 for holo-S100A1 and holo-S100A1-Hcy, respectively. The anisotropy of the overall tumbling in apo-S100A1 is less pronounced and equal to 0.92 ± 0.02. The averaged isotropic rotational correlation time $[\tau_R = (2D_x + 2D_y + 2D_z)^{-1}]$ is equal to 9.50 ± 0.08 and 9.27 ± 0.20 ns for holo-S100A1 and holo-S100A1-Hcy, respectively, which are typical for ∼20 kDa globular proteins and correspond well to the results obtained for other proteins from the S100 family.[14,65−68] Comparison of the apo and holo forms reveals that overall tumbling of holo forms is ∼10% slower. It should not be surprising in the light of larger molecular inertia moments of holo forms (cf. Table S1 of the Supporting Information).

Of five residue-specific parameters describing the local mobility of the backbone amide N−H vectors within the frame of the extended model-free approach, S^2 $(=S_f^2S_s^2)$ and R_{ex} are of special importance. The former describes restrictions imposed on motions much faster than the overall protein diffusion (picosecond time scale), and the latter allows detection of much slower motions, but fast enough to average chemical shifts of the exchanging sites (usually on the microsecond to millisecond time scale). Site-specific values of those parameters can reveal local changes in dynamics caused by the thionylation and calcium loading for both studied proteins when compared with corresponding values in apo-S100A1.[14] However, differences in the mobility of the protein structural elements (helices and loops) on the picosecond time scale become much more evident when the weighted means of S^2 values determined for the residues building them are compared.

The S^2 values averaged over structural elements presented in Figure 3 indicate that the helices are always the most rigid segments of the studied proteins (full profiles of site-specific S^2 values are given in Figure S3 of the Supporting Information).

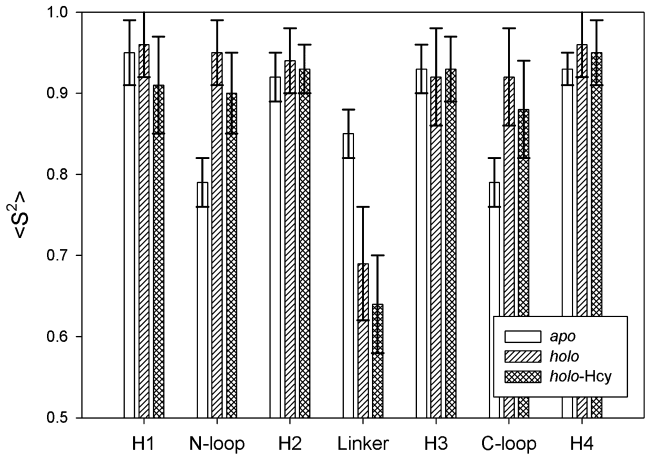

Figure 3. Weighted means of generalized order parameter values $\langle S^2 \rangle$ with corresponding error bars for amino acid residues in various structural elements of human holo-S100A1 and holo-S100A1-Hcy proteins compared with corresponding values obtained for apo-S100A1.[14] Relaxation data were analyzed assuming fully anisotropic overall tumbling[57] and extended model-free spectral density functions.[54]

The rigidity of both binding loops in the holo forms is comparable to that of helices. On the other hand, the linker is the most flexible part of the molecule, much more flexible than in the apo form. In the holo forms, residues involved in chemical exchange processes monitored by the R_{ex} parameter (Figure 4) are predominantly located in helices I and II and the linker in contrast to those most affected by exchange processes, the N-terminal binding loop in the apo form.

Residues of binding loops differ in their dynamic behavior between the holo and apo forms. In the latter structure, the residues located in the binding loops display intense mobility on the picosecond time scale comparable to that of the linker. Moreover, they show the exchange terms are the largest in the N-terminal loop. Therefore, calcium binding imposes a restriction on the mobility of residues comprising binding loops on fast and slow time scales. On the other hand, the mobility of the linker, on both time scales, and of large parts of helices I and II on the slow time scale becomes more pronounced in the holo forms.

The obtained model parameters reproduce well input experimental data. The plot of calculated versus experimental R_2/R_1 ratios is given in Figure S4 of the Supporting Information.

DISCUSSION

Impact of Calcium Binding on the Human S100A1 Structure and Its Backbone Dynamics. The structural transition in the human S100A1 protein induced by calcium binding is strictly similar to that observed in rat S100A1[2,69] and characteristic for the majority of S100 proteins:[65,70] helix III changes its orientation by ∼100° (cf. Table 2 and Figure 5), which leads to the creation of a large hydrophobic cleft on the surface of the protein comprising the residues situated in the linker, helix III, and helix IV. The target proteins bind to this region of holo-S100A1.[71,72]

The authors of studies of rat S100A1[2,69] have concluded that elongation of helix IV at its C-terminus is an additional structural change induced by calcium binding in the protein. A similar conclusion has been drawn from studies of human S100A5.[65] In human apo-S100A1,[14] we have found one additional turn in helix IV versus the number reported for the rat apoprotein,[69] but the residues participating in its formation (Asn 87−Trp 90) are in equilibrium between helical (3_{10}-helix) and nonhelical conformations. In the holo forms of S100A1 presented here, the equilibrium is shifted toward the α-helical conformation.

As could be expected, the striking difference in the dynamics of apo-S100A1 and holo-S100A1 proteins is the significant restriction of motion of both calcium binding loops. S^2 values averaged over structural motifs are larger for calcium binding loops in holo-S100A1 (cf. Figure 3). In the calcium-bound form, those structural elements previously mobile on the subnanosecond time scale become as rigid as helices. In other words, quite expectedly calcium binding imposes restriction on fast motions of the loops. Additionally, the linker region in holo-S100A1 becomes more mobile, and thionylation of Cys 85 enhances this effect. The latter phenomenon can be explained by possible interactions between the attached homocysteine and residues within the linker (cf. Figure 2B). Moreover, the analysis of differences in R_{ex} terms for those two proteins reveals that calcium binding restricts the mobility of the S100-specific calcium binding loop. There is another feature that characterizes studied holoprotein forms, namely the significant

dx.doi.org/10.1021/bi3015407 | Biochemistry 2013, 52, 1149−1159

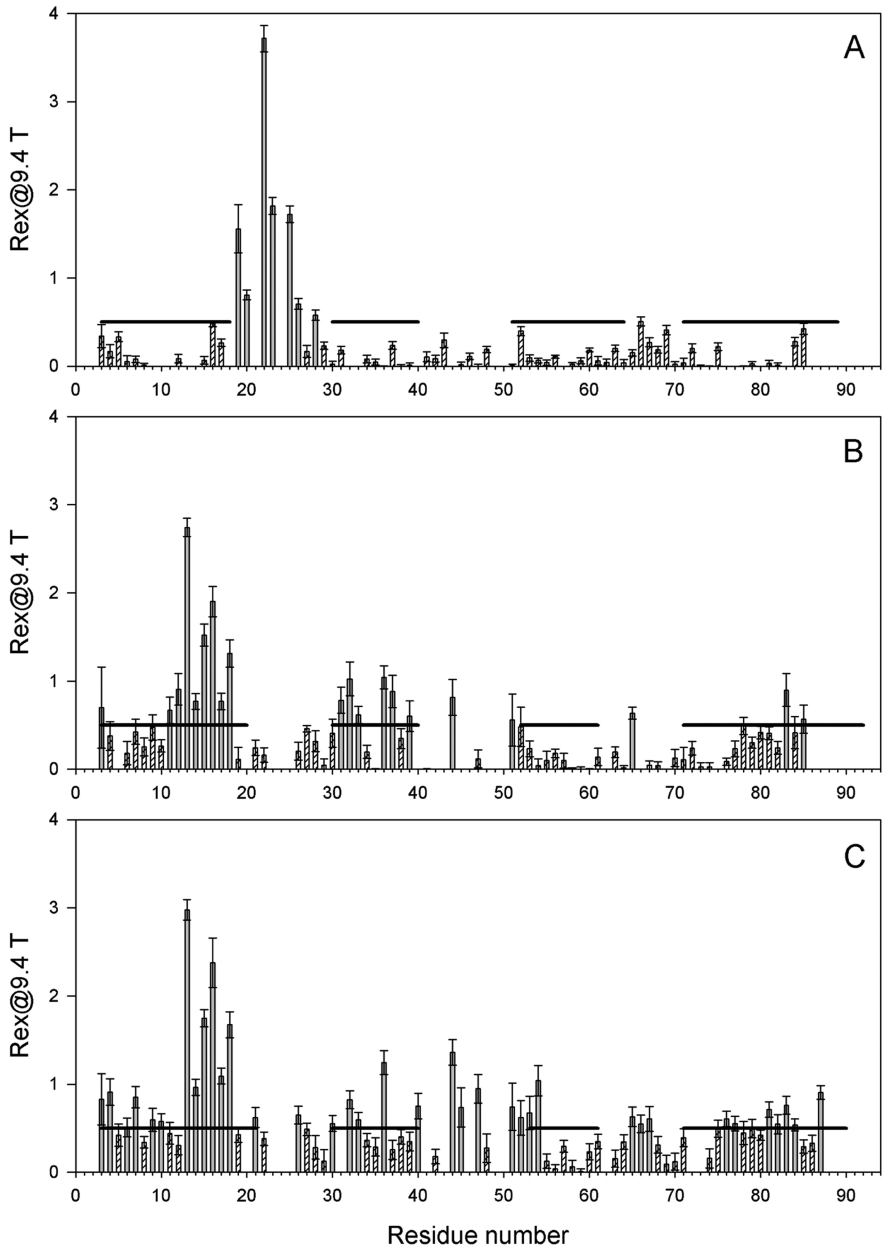

Figure 4. Data (vertical bars) for exchange terms R_{ex} at 9.4 T with corresponding error bars for human apo-S100A1 (A), holo-S100A1 (B), and holo-S100A1-Hcy (C) vs residue number. Insignificant R_{ex} values of <0.5 s^{-1} and, therefore, close to their accuracy are shown as hatched bars. The horizontal lines indicate positions of four helices in EF-hand motifs.

increase in the exchange terms of helices I and II in comparison with those of the apo form. This effect has not been reported for any S100 proteins until now. It points to the increased mobility on the microsecond to millisecond time scale of secondary structure elements that usually remain rigid. This behavior can be a hallmark of the target binding site as recently reported for the S100A6 complex with a fragment of the C-terminal domain of Siah-1 protein.[3] It was observed that complex formation resulted in both chemical shift perturbation in the H/N correlation spectrum and the broadening or disappearance of numerous cross-peaks corresponding to several regions of S100A6, including most of the residues within helix I. It can also correlate with the increased rates of exchange of several amide protons with solvent within helices I and II of human[73] and rat[74] S100B proteins.

Comparison of Holo-S100A1 Structures. Until now, there have been three available structures of holo-S100A1 proteins: rat (PDB entry 1ZFS)[2] and human (PDB entry 2LP3) and human thionylated with homocysteine (PDB entry 2LP2) (the latter two presented in this paper). All these structures, determined by NMR methods, are very similar. The rmsd values calculated for backbone atoms of residues Glu 5−Cys 85 in 1ZFS/2LP3, 1ZFS/2LP2, and 2LP2/2LP3 structure pairs equal 1.92 ± 0.20, 2.24 ± 0.11, and 1.63 ± 0.09 Å, respectively. The positions of secondary structure elements as well as mutual orientations of helices (see Table 2) are also very similar in those three structures. The only structural difference is visible in the linker region (residues Leu 41−Asp 50). It does not contain any elements of secondary structure in rat and human holo-S100A1 proteins, while in holo-S100A1-Hcy, an α-helical segment consisting of Gly 43−Gln 46 has been found.

dx.doi.org/10.1021/bi3015407 | *Biochemistry* 2013, 52, 1149−1159

Table 2. Angles (in degrees) among Helices I–IV in Human and Rat S100A1 Structures[a]

helices	human apo-S100A1[b]	rat holo-S100A1[c]	human holo-S100A1[d]	human holo-S100A1-Hcy[e]
I → II	133 ± 1	132 ± 1	132 ± 2	139 ± 1
I → IV	117 ± 1	131 ± 2	119 ± 2	130 ± 1
II → IV	−34 ± 1	−29 ± 1	−26 ± 3	−35 ± 1
I → I′	−144 ± 2	−157 ± 3	−158 ± 2	−154 ± 1
IV → IV′	151 ± 1	152 ± 3	144 ± 6	149 ± 1
III → IV	−167 ± 2	121 ± 2	130 ± 4	112 ± 2

[a]Interhelical angles were calculated using interhlx (K. Yap, University of Toronto, Toronto, ON). The sign of the interhelical angle was chosen according to convention proposed in ref 78. [b]Taken from the NMR structure (PDB entry 2L0P). [c]Taken from the NMR structure (PDB entry 1ZFS). [d]Taken from the NMR structure (PDB entry 2LP3), from this work. [e]Taken from the NMR structure (PDB entry 2LP2), from this work.

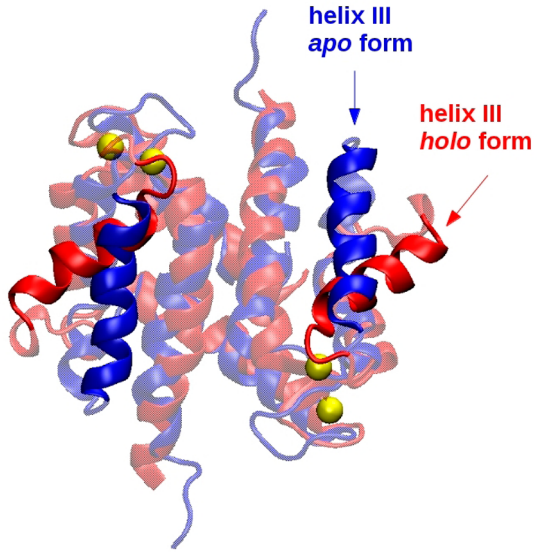

Figure 5. Comparison of most representative structures for human holo-S100A1 (red) and apo-S100A1 (blue) proteins. Calcium ions are represented as yellow spheres.

Nevertheless, we believe that it is simply more populated because in all these proteins the linker region is very flexible (see Figure 3). The existence of a short α-helix in the linker region has been found in all crystallographic structures of calcium-loaded S100 proteins.[75−77] Moreover, the chemical shift index (CSI) values of Cα nuclei obtained for all S100A1 proteins discussed here indicate that residues 42−46 (42−45 in rat S100A1) are likely to adopt the α-helical conformation (cf. Figure S5 of the Supporting Information).

The results presented here show that protein thionylation is not reflected in any significant changes in the structure or dynamics of its holo form. Therefore, the rationale for the increase in the protein affinity for calcium due to the thionylation of Cys 85 should be searched in conformational changes in its apo form.

Therefore, it seems obvious that we should investigate this problem by thoroughly analyzing the structure of apo-S100A1-Hcy. Unfortunately, the signal dispersion in NMR spectra of this protein is very poor, precluding spectral assignments at the level allowing for the precise structure determination. Nevertheless, at least partial assignment of a number of resonances was possible. It allowed us to identify C/H correlations for several aromatic moieties and calculate CSP values caused either by calcium binding or by thionylation of the protein. The aromatic $^{1}H-^{13}C$ HSQC spectra, which can be regarded as fingerprints of the hydrophobic core arrangement, are virtually identical for both studied holoproteins (S100A1 and S100A1-Hcy) and the apo form of S100A1-Hcy, while the corresponding spectrum of native apo-S100A1 markedly differs from them. Visual inspection of superpositions of selected pairs of 2D aromatic $^{1}H-^{13}C$ HSQC spectra (Figure S6 of the Supporting Information) confirms this statement. Selected CSP values of aromatic C/H cross-peaks and the Nε1/Hε1 side chain Trp residue are large and similar for apo-S100A1/holo-S100A1 and apo-S100A1/apo-S100A1-Hcy pairs. On the other hand, they are much smaller for the apo-S100A1-Hcy/holo-S100A1-Hcy pair (cf. Table S3 of the Supporting Information). One can conclude that the rearrangement of hydrophobic side chains of aromatic residues caused by protein thionylation reflected by the aromatic C/H correlation spectrum of apo-S100A1-Hcy is similar to that resulting from binding of calcium to S100A1. This conclusion is in line with our previous finding that Cys 85 thionylation stabilizes the C-terminal part of helix IV in S100A1 protein[68] as does calcium binding.

CONCLUSIONS

Loading of S100A1 protein with calcium results in stabilization of the C-terminal part of α-helix IV in addition to drastic reorientation of helix III. As could be expected, the calcium binding loops are much more rigid in the holo form of the protein.

Quite surprisingly, helices I and II and, in particular, the linker region in the holo form are more flexible than in the apo form. It can be of functional importance facilitating molecular recognition of the protein target molecules.

Neither the structure nor the dynamics of holo-S100A1 are perceptibly affected by protein thionylation. That leads to the following important conclusion: the observed increase in the affinity of S100A1 for calcium upon its Cys 85 thionylation results generally from conformational changes in the apo form of the protein that seem to arise from rearrangement of aromatic residues constituting its hydrophobic core.

ASSOCIATED CONTENT

Supporting Information

Detailed information about the structure and dynamics of studied proteins (three tables and six figures). This material is available free of charge via the Internet at http://pubs.acs.org.

Accession Codes

The coordinates for the human holo-S100A1 and holo-S100A1-Hcy structures have been deposited in the Protein Data Bank (entries 2LP3 and 2LP2, respectively). The ^{1}H, ^{13}C, and ^{15}N resonance assignments and ^{15}N magnetic relaxation data have been deposited in the BioMagResBank (entries 18231 and 18230, respectively).

AUTHOR INFORMATION

Corresponding Author

*Phone: +48 22 8220211 421. E-mail: lyam@chem.uw.edu.pl.

Present Addresses

‖Faculty of Chemistry, Warsaw University, Pasteura 1, 02-093 Warsaw, Poland.

[⊥]Department for NMR-based Structural Biology, Max Planck Institute for Biophysical Chemistry, Göttingen, Germany.

Author Contributions

K.R.-B. and M.B. contributed equally to this work.

Funding

This work was supported by grants from the Ministry of Science and Higher Education (N301/031234 and N301/122438) and the Iuventus Plus program (Project 0193/IP1/2011/71 to Ł.J.).

Notes

The authors declare no competing financial interest.

■ ACKNOWLEDGMENTS

We are grateful to Prof. Wiktor Koźmiński from Warsaw University and Dr. Igor Zhukov (National Institute of Chemistry, Ljubljana, Slovenia) for making high-field NMR spectrometers available to us.

■ ABBREVIATIONS

CPMG, Carr−Purcell−Meiboom−Gill; CSI, chemical shift index; CSP, chemical shift perturbation; DSS-d_4, 3-(trimethylsilyl)-2,2,3,3-tetradeuteropropionic acid sodium salt; EDTA, ethylenediaminetetraacetic acid; HSQC, heteronuclear single-quantum coherence; HPLC, high-performance liquid chromatography; rmsd, root-mean-square deviation; SD, standard deviation; Tris-d_{11}, perdeuterated 2-amino-2-(hydroxymethyl)-1,3-propanediol.

■ REFERENCES

(1) Santamaria-Kisiel, L., Rintala-Dempsey, A. C., and Shaw, G. S. (2006) Calcium-dependent and -independent interactions of the S100 protein family. *Biochem. J. 396*, 201−214.

(2) Wright, N. T., Varney, K. M., Ellis, K. C., Markowitz, J., Gitti, R. K., Zimmer, D. B., and Weber, D. J. (2005) The three-dimensional solution structure of Ca^{2+}-bound S100A1 as determined by NMR spectroscopy. *J. Mol. Biol. 353*, 410−426.

(3) Lee, Y. T., Dimitrova, Y. N., Schneider, G., Ridenour, W. B., Bhattacharya, S., Soss, S. E., Caprioli, R. M., Filipek, A., and Chazin, W. J. (2008) Structure of the S100A6 complex with a fragment from the C-terminal domain of Siah-1 interacting protein: A novel mode for S100 protein target recognition. *Biochemistry 47*, 10921−10932.

(4) Zimmer, D. B., Chaplin, J., Baldwin, A., and Rast, M. (2005) S100-mediated signal transduction in the nervous system and neurological diseases. *Cell. Mol. Biol. (Sarreguemines, Fr., Online) 51*, 201−214.

(5) Heizmann, C. W., Fritz, G., and Schafer, B. W. (2002) S100 proteins: Structure, functions and pathology. *Front. Biosci. 7*, d1356−d1368.

(6) Rohde, D., Ritterhoff, J., Voelkers, M., Katus, H. A., Parker, T. G., and Most, P. (2010) S100A1: A multifaceted therapeutic target in cardiovascular disease. *Journal of Cardiovascular Translational Research 3*, 525−537.

(7) Kraus, C., Rohde, D., Weidenhammer, C., Qiu, G., Pleger, S. T., Voelkers, M., Boerries, M., Remppis, A., Katus, H. A., and Most, P. (2009) S100A1 in cardiovascular health and disease: Closing the gap between basic science and clinical therapy. *J. Mol. Cell. Cardiol. 47*, 445−455.

(8) Goch, G., Vdovenko, S., Kozlowska, H., and Bierzynski, A. (2005) Affinity of S100A1 protein for calcium increases dramatically upon glutathionylation. *FEBS J. 272*, 2557−2565.

(9) Ghezzi, P., Bonetto, V., and Fratelli, M. (2005) Thiol-disulfide balance: From the concept of oxidative stress to that of redox regulation. *Antioxid. Redox Signaling 7*, 964−972.

(10) Dalle-Donne, I., Rossi, R., Colombo, G., Giustarini, D., and Milzani, A. (2009) Protein S-glutathionylation: A regulatory device from bacteria to humans. *Trends Biochem. Sci. 34*, 85−96.

(11) Ghezzi, P., and Di Simplicio, P. (2009) Protein glutationylation. In *Redox signaling and regulation in biology and medicine* (Jacob, C., and Winyard, P. C., Eds.) pp 123−141, Wiley-VCH, Weinheim, Germany.

(12) Palmer, A. G., III (2004) NMR characterization of the dynamics of biomacromolecules. *Chem. Rev. 104*, 3623−3640.

(13) Morin, S. (2011) A practical guide to protein dynamics from ^{15}N spin relaxation in solution. *Prog. Nucl. Magn. Reson. Spectrosc. 59*, 245−262.

(14) Nowakowski, M., Jaremko, L., Jaremko, M., Zhukov, I., Belczyk, A., Bierzynski, A., and Ejchart, A. (2011) Solution NMR structure and dynamics of human apo-S100A1 protein. *J. Struct. Biol. 174*, 391−399.

(15) Finkelstein, J. D. (1998) The metabolism of homocysteine: Pathways and regulation. *Eur. J. Pediatr. 157* (Suppl.2), S40−S44.

(16) Hultberg, B., Andersson, A., and Isaksson, A. (1998) Protein binding of homocysteine and other thiols in HeLa cell cultures after addition of homocysteine and copper ions. *Clin. Chim. Acta 269*, 175−184.

(17) Mansoor, M. A., Guttormsen, A. B., Fiskerstrand, T., Refsum, H., Ueland, P. M., and Svardal, A. M. (1993) Redox status and protein binding of plasma aminothiols during the transient hyperhomocysteinemia that follows homocysteine administration. *Clin. Chem. 39*, 980−985.

(18) Nygard, O., Nordrehaug, J. E., Refsum, H., Ueland, P. M., Farstad, M., and Vollset, S. E. (1997) Plasma homocysteine levels and mortality in patients with coronary artery disease. *N. Engl. J. Med. 337*, 230−236.

(19) Glushchenko, A. V., and Jacobsen, D. W. (2007) Molecular targeting of proteins by L-homocysteine: Mechanistic implications for vascular disease. *Antioxid. Redox Signaling 9*, 1883−1898.

(20) Kessler, H., Bleich, S., Falkai, P., and Supprian, T. (2003) [Homocysteine and dementia]. *Fortschr. Neurol., Psychiatr. Ihrer Grenzgeb. 71*, 150−156.

(21) Morris, M. S. (2003) Homocysteine and Alzheimer's disease. *Lancet Neurol. 2*, 425−428.

(22) Bolewska, K., Kozlowska, H., Goch, G., Mikołajek, B., and Bierzynski, A. (1997) Molecular cloning and expression in *Escherichia coli* of a gene coding for bovine S100A1 protein and its Glu32 Gln and Glu73 Gln mutants. *Acta Biochim. Pol. 44*, 275−284.

(23) Dixon, M., and Webb, E. C. (1961) Enzyme fractionation by salting-out: A theoretical note. *Adv. Protein Chem. 16*, 197−219.

(24) Falconer, J. S., Jenden, D. J., and Taylor, D. B. (1953) The application of solubility measurements to the study of complex protein solutions and to the isolation of individual proteins. *Discuss. Faraday Soc. 13*, 40−50.

(25) Baldisseri, D. M., Rustandi, R. R., Zhang, Z., Tang, C., Bair, C. L., Landar, A., Zimmer, D. B., and Weber, D. J. (1999) ^{1}H, ^{13}C and ^{15}N NMR sequence-specific resonance assignments for rat apo-S100A1($\alpha\alpha$). *J. Biomol. NMR 14*, 91−92.

(26) Marion, D., Ikura, M., Tschudin, R., and Bax, A. (1989) Rapid recording of 2D NMR spectra without phase cycling. Application to the study of hydrogen exchange in proteins. *J. Magn. Reson. 85*, 393−399.

(27) Kay, L. E., Keifer, P., and Saarinen, T. (1992) Pure absorption gradient enhanced heteronuclear single quantum correlation spectroscopy with improved sensitivity. *J. Am. Chem. Soc. 114*, 10663−10665.

(28) Wishart, D. S., Bigam, C. G., Yao, C. G., Abildgaad, F., Dyson, H. J., Oldfield, E., Markley, J. L., and Sykes, B. D. (1995) ^{1}H, ^{13}C and ^{15}N chemical shift referencing in biomolecular NMR. *J. Biomol. NMR 6*, 135−140.

(29) Delaglio, F., Grzesiek, S., Vuister, G. W., Zhu, G., Pfeifer, J., and Bax, A. (1995) NMRPipe: A multidimensional spectral processing system based on UNIX pipes. *J. Biomol. NMR 6*, 277−293.

(30) Keller, R. L. J. (2004) The computer aided resonance assignment tutorial. http://www.cara.nmr.ch.

(31) Goddard, T. D., and Kneller, D. G. (2010) *SPARKY3*, University of California, San Francisco.

(32) Muhandiram, D. R., and Kay, L. E. (1994) Gradient-enhanced triple-resonance three-dimensional NMR experiments with improved sensitivity. *J. Magn. Reson., Ser. B 103*, 203−216.
(33) Ikura, M., Kay, L. E., and Bax, A. (1990) A novel approach for sequential assignment of ^{1}H, ^{13}C, and ^{15}N spectra of proteins: Heteronuclear triple-resonance three-dimensional NMR spectroscopy. Application to calmodulin. *Biochemistry 29*, 4659−4667.
(34) Bax, A., and Ikura, M. (1991) An efficient 3D NMR technique for correlating the proton and ^{15}N backbone amide resonances with the α-carbon of the preceding residue in uniformly ^{15}N/^{13}C enriched proteins. *J. Biomol. NMR 1*, 99−104.
(35) Wittekind, M., and Mueller, L. (1993) HNCACB, a high-sensivity 3D NMR experiment to correlate amide proton and nitrogen resonances with the α- and β-carbon resonances in proteins. *J. Magn. Reson., Ser. B 101*, 201−205.
(36) Grzesiek, S., and Bax, A. (1992) Correlating backbone amide and side chain resonances in larger proteins by multiple relayed triple resonance NMR. *J. Am. Chem. Soc. 114*, 6291−6293.
(37) Lohr, F., and Ruterjans, H. (1995) A new triple-resonance experiment for the sequential assignment of backbone resonances in proteins. *J. Biomol. NMR 6*, 189−197.
(38) Zhang, O., Kay, L. E., Olivier, J. P., and Forman-Kay, J. D. (1994) Backbone ^{1}H and ^{15}N resonance assignments of the N-terminal SH3 domain of drk in folded and unfolded states using enhanced-sensitivity pulsed field gradient NMR techniques. *J. Biomol. NMR 4*, 845−858.
(39) Grzesiek, S., Anglister, J., and Bax, A. (1993) Correlation of backbone amide and aliphatic side-chain resonances in ^{13}C/^{15}N-enriched proteins by isotropic mixing of ^{13}C magnetization. *J. Magn. Reson., Ser. B 101*, 114−119.
(40) Grzesiek, S., and Bax, A. (1993) Amino acid type determination in the sequential assignment procedure of uniformly ^{13}C/^{15}N-enriched proteins. *J. Biomol. NMR 3*, 185−204.
(41) Bax, A., Clore, G. M., and Gronenborn, A. M. (1990) ^{1}H-^{1}H correlation via isotropic mixing of ^{13}C magnetization: A new three-dimensional approach for assigning ^{1}H and ^{13}C spectra of ^{13}C-enriched proteins. *J. Magn. Reson. 88*, 425−431.
(42) Muhandiram, D. R., Farrow, N. A., Xu, G.-Y., Smallcombe, S. H., and Kay, L. E. (1993) A gradient ^{13}C NOESY-HSQC experiment for recording NOESY spectra of ^{13}C-labeled proteins dissolved in H_2O. *J. Magn. Reson., Ser. B*, 317−321.
(43) Yamazaki, T., Forman-Kay, J. D., and Kay, L. E. (1993) Two-dimensional NMR experiments for correlating ^{13}Cβ and ^{1}Hδ/ε chemical shifts of aromatic residues in ^{13}C-labeled proteins via scalar couplings. *J. Am. Chem. Soc. 115*, 11054−11055.
(44) Farrow, N. A., Muhandiram, R., Singer, A. U., Pascal, S. M., Kay, C. M., Gish, G., Shoelson, S. E., Pawson, T., Forman-Kay, J. D., and Kay, L. E. (1994) Backbone dynamics of a free and phosphopeptide-complexed Src homology 2 domain studied by ^{15}N NMR relaxation. *Biochemistry 33*, 5984−6003.
(45) Kay, L. E., Nicholson, L. K., Delaglio, F., Bax, A., and Torchia, D. A. (1992) Pulse schemes for removal of the effects of cross correlation between dipolar and chemical-shift anisotropy relaxation mechanisms on the measurement of heteronuclear T1 and T2 values in proteins. *J. Magn. Reson. 97*, 359−375.
(46) Fushman, D. (2003) Determination of protein dynamics using ^{15}N relaxation measurements. In *BioNMR in Drug Research* (Zerbe, O., Ed.) pp 283−308, Wiley-VCH, Weinheim, Germany.
(47) Guntert, P., Mumenthaler, C., and Wuthrich, K. (1997) Torsion angle dynamics for NMR structure calculation with the new program DYANA. *J. Mol. Biol. 273*, 283−298.
(48) Herrmann, T., Guntert, P., and Wuthrich, K. (2002) Protein NMR structure determination with automated NOE-identification in the NOESY spectra using the new software ATNOS. *J. Biomol. NMR 24*, 171−189.
(49) Guntert, P., Qian, Y. Q., Otting, G., Muller, M., Gehring, W., and Wuthrich, K. (1991) Structure determination of the Antp (C39−S) homeodomain from nuclear magnetic resonance data in solution using a novel strategy for the structure calculation with the programs DIANA, CALIBA, HABAS and GLOMSA. *J. Mol. Biol. 217*, 531−540.
(50) Berjanskii, M. V., Neal, S., and Wishart, D. S. (2006) PREDITOR: A web server for predicting protein torsion angle restraints. *Nucleic Acids Res. 34*, W63−W69.
(51) Schwieters, C. D., Kuszewski, J. J., Tjandra, N., and Clore, G. M. (2003) The Xplor-NIH NMR molecular structure determination package. *J. Magn. Reson. 160*, 65−73.
(52) Laskowski, R. A., Rullmannn, J. A., MacArthur, M. W., Kaptein, R., and Thornton, J. M. (1996) AQUA and PROCHECK-NMR: Programs for checking the quality of protein structures solved by NMR. *J. Biomol. NMR 8*, 477−486.
(53) Vriend, G. (1990) WHAT IF: A molecular modeling and drug design program. *J. Mol. Graphics 8* (29), 52−56.
(54) Clore, G. M., Szabo, A., Bax, A., Kay, L. E., Driscoll, P. C., and Gronenborn, A. M. (1990) Deviations from the simple two-parameter model-free approach to the interpretation of nitrogen-15 nuclear magnetic relaxation of proteins. *J. Am. Chem. Soc. 112*, 4989−4991.
(55) Baber, J. L., Szabo, A., and Tjandra, N. (2001) Analysis of slow interdomain motion of macromolecules using NMR relaxation data. *J. Am. Chem. Soc. 123*, 3953−3959.
(56) Tjandra, N., Kuboniwa, H., Ren, H., and Bax, A. (1995) Rotational dynamics of calcium-free calmodulin studied by ^{15}N-NMR relaxation measurements. *Eur. J. Biochem. 230*, 1014−1024.
(57) Woessner, D. E. (1962) Nuclear spin relaxation in ellipsoid undergoing rotational Brownian motion. *J. Chem. Phys. 37*, 647−654.
(58) Ottinger, M., and Bax, A. (1998) Determination of relative N-HN, N-C′, Ca-C′, and Ca-Ha effective bond lengths in a protein by NMR in a dilute liquid crystalline phase. *J. Am. Chem. Soc. 120*, 12334−12341.
(59) Yao, L., Grishaev, A., Cornilescu, G., and Bax, A. (2010) Site-specific backbone amide ^{15}N chemical shift anisotropy tensors in a small protein from liquid crystal and cross-correlated relaxation measurements. *J. Am. Chem. Soc. 132*, 4295−4309.
(60) Alexandrescu, A. T., and Shortle, D. (1994) Backbone dynamics of a highly disordered 131 residue fragment of staphylococcal nuclease. *J. Mol. Biol. 242*, 527−546.
(61) Brutscher, B., Bruschweiler, R., and Ernst, R. R. (1997) Backbone dynamics and structural characterization of the partially folded A state of ubiquitin by ^{1}H, ^{13}C, and ^{15}N nuclear magnetic resonance spectroscopy. *Biochemistry 36*, 13043−13053.
(62) Press, W. H., Flannery, B. P., Teukolsky, S. A., and Vetterling, W. T. (1986) in *Numerical recipes. The art of scientific computing*, Cambridge University Press, Cambridge, U.K.
(63) Martin, O. A., Villegas, M. E., Vila, J. A., and Scheraga, H. A. (2010) Analysis of ^{13}Cα and ^{13}Cβ chemical shifts of cysteine and cystine residues in proteins: A quantum chemical approach. *J. Biomol. NMR 46*, 217−225.
(64) Sharma, D., and Rajarathnam, K. (2000) ^{13}C NMR chemical shifts can predict disulfide bond formation. *J. Biomol. NMR 18*, 165−171.
(65) Bertini, I., Das Gupta, S., Hu, X., Karavelas, T., Luchinat, C., Parigi, G., and Yuan, J. (2009) Solution structure and dynamics of S100A5 in the apo and Ca^{2+}-bound states. *J. Biol. Inorg. Chem. 14*, 1097−1107.
(66) Dutta, K., Cox, C. J., Basavappa, R., and Pascal, S. M. (2008) ^{15}N relaxation studies of Apo-Mts1: A dynamic S100 protein. *Biochemistry 47*, 7637−7647.
(67) Inmam, K. G., Baldisseri, D. M., Miller, K. E., and Weber, D. J. (2001) Backbone dynamics of the calcium-signaling protein apo-S100B as determined by ^{15}N NMR relaxation. *Biochemistry 40*, 3439−3448.
(68) Zhukov, I., Ejchart, A., and Bierzynski, A. (2008) Structural and motional changes induced in apo-S100A1 protein by the disulfide formation between its Cys 85 residue and β-mercaptoethanol. *Biochemistry 47*, 640−650.
(69) Rustandi, R. R., Baldisseri, D. M., Inman, K. G., Nizner, P., Hamilton, S. M., Landar, A., Zimmer, D. B., and Weber, D. J. (2002)

Three-dimensional solution structure of the calcium-signaling protein apo-S100A1 as determined by NMR. *Biochemistry 41*, 788−796.
(70) Otterbein, L. R., Kordowska, J., Witte-Hoffmann, C., Wang, C. L., and Dominguez, R. (2002) Crystal structures of S100A6 in the Ca^{2+}-free and Ca^{2+}-bound states: The calcium sensor mechanism of S100 proteins revealed at atomic resolution. *Structure 10*, 557−567.
(71) Wright, N. T., Prosser, B. L., Varney, K. M., Zimmer, D. B., Schneider, M. F., and Weber, D. J. (2008) S100A1 and calmodulin compete for the same binding site on ryanodine receptor. *J. Biol. Chem. 283*, 26676−26683.
(72) Wright, N. T., Cannon, B. R., Wilder, P. T., Morgan, M. T., Varney, K. M., Zimmer, D. B., and Weber, D. J. (2009) Solution structure of S100A1 bound to the CapZ peptide (TRTK12). *J. Mol. Biol. 386*, 1265−1277.
(73) Smith, S. P., and Shaw, G. S. (1997) Assignment and secondary structure of calcium-bound human S100B. *J. Biomol. NMR 10*, 77−88.
(74) Drohat, A. C., Baldisseri, D. M., Rustandi, R. R., and Weber, D. J. (1998) Solution structure of calcium-bound rat S100B($\beta\beta$) as determined by nuclear magnetic resonance spectroscopy. *Biochemistry 37*, 2729−2740.
(75) Koch, M., and Fritz, G. (2012) The structure of Ca^{2+}-loaded S100A2 at 1.3-Å resolution. *FEBS J. 279*, 1799−1810.
(76) Rety, S., Osterloh, D., Arie, J. P., Tabaries, S., Seeman, J., Russo-Marie, F., Gerke, V., and Lewit-Bentley, A. (2000) Structural basis of the Ca^{2+}-dependent association between S100C (S100A11) and its target, the N-terminal part of annexin I. *Structure 8*, 175−184.
(77) Gingras, A. R., Basran, J., Prescott, A., Kriajevska, M., Bagshaw, C. R., and Barsukov, I. L. (2008) Crystal structure of the Ca^{2+}-form and Ca^{2+}-binding kinetics of metastasis-associated protein, S100A4. *FEBS Lett. 582*, 1651−1656.
(78) Drohat, A. C., Amburgey, J. C., Abildgaard, F., Starich, M. R., Baldisseri, D., and Weber, D. J. (1996) Solution structure of rat apo-S100B($\beta\beta$) as determined by NMR spectroscopy. *Biochemistry 35*, 11577−11588.